

Optimization of Early Response Monitoring and Prediction of Cancer Antiangiogenesis Therapy via Noninvasive PET Molecular Imaging Strategies of Multifactorial Bioparameters

Xiao Bao*, Ming-Wei Wang[✉], Jian-Min Luo, Si-Yang Wang, Yong-Ping Zhang, Ying-Jian Zhang

Department of Nuclear Medicine, Fudan University Shanghai Cancer Center; Department of Oncology, Shanghai Medical College, Fudan University; Center for Biomedical Imaging, Fudan University; Shanghai Engineering Research Center for Molecular Imaging Probes, Shanghai 200032, China.

* Current address (Xiao Bao): Department of Radiology, Shanghai Pulmonary Hospital, Tongji University School of Medicine, 507 Zhengmin Road, Shanghai 200433, China.

[✉] Corresponding author: Ming-Wei Wang, Department of Nuclear Medicine, Fudan University Shanghai Cancer Center, Shanghai 200032, China. Phone/Fax: +86-21-64175590; E-Mail: wang.mingwei88@163.com.

© Ivyspring International Publisher. Reproduction is permitted for personal, noncommercial use, provided that the article is in whole, unmodified, and properly cited. See <http://ivyspring.com/terms> for terms and conditions.

Received: 2015.09.20; Accepted: 2016.07.30; Published: 2016.09.10

Abstract

Objective: Antiangiogenesis therapy (AAT) has provided substantial benefits regarding improved outcomes and survival for suitable patients in clinical settings. Therefore, the early definition of therapeutic effects is urgently needed to guide cancer AAT. We aimed to optimize the early response monitoring and prediction of AAT efficacy, as indicated by the multi-targeted anti-angiogenic drug sunitinib in U87MG tumors, using noninvasive positron emission computed tomography (PET) molecular imaging strategies of multifactorial bioparameters.

Methods: U87MG tumor mice were treated via intragastric injections of sunitinib (80 mg/kg) or vehicle for 7 consecutive days. Longitudinal MicroPET/CT scans with ¹⁸F-FDG, ¹⁸F-FMISO, ¹⁸F-ML-10 and ¹⁸F-Alfatide II were acquired to quantitatively measure metabolism, hypoxia, apoptosis and angiogenesis on days 0, 1, 3, 7 and 13 following therapy initiation. Tumor tissues from a dedicated group of mice were collected for immunohistochemical (IHC) analysis of key biomarkers (Glut-1, CA-IX, TUNEL, $\alpha_v\beta_3$ and CD31) at the time points of PET imaging. The tumor sizes and mouse weights were measured throughout the study. The tumor uptake (ID%/g_{max}), the ratios of the tumor/muscle (T/M) for each probe, and the tumor growth ratios (TGR) were calculated and used for statistical analyses of the differences and correlations.

Results: Sunitinib successfully inhibited U87MG tumor growth with significant differences in the tumor size from day 9 after sunitinib treatment compared with the control group ($P < 0.01$). The uptakes of ¹⁸F-FMISO (reduced hypoxia), ¹⁸F-ML-10 (increased apoptosis) and ¹⁸F-Alfatide II (decreased angiogenesis) in the tumor lesions significantly changed during the early stage (days 1 to 3) of sunitinib treatment; however, the uptake of ¹⁸F-FDG (increased glucose metabolism) was significantly different during the late stage. The PET imaging data of each probe were all confirmed via ex vivo IHC of the relevant biomarkers. Notably, the PET imaging of ¹⁸F-Alfatide II and ¹⁸F-FMISO was significantly correlated (all $P < 0.05$) with TGR, whereas the imaging of ¹⁸F-FDG and ¹⁸F-ML-10 was not significantly correlated with TGR.

Conclusion: Based on the tumor uptake of the PET probes and their correlations with MVD and TGR, ¹⁸F-Alfatide II PET may not only monitor the early response but also precisely predict the therapeutic efficacy of the multi-targeted, anti-angiogenic drug sunitinib in U87MG tumors. In conclusion, it is feasible to optimize the early response monitoring and efficacy prediction of

cancer AAT using noninvasive PET molecular imaging strategies of multifactorial bioparameters, such as angiogenesis imaging with ¹⁸F-Alfatide II, which represents an RGD-based probe.

Key words: Antiangiogenesis therapy; PET; Molecular imaging probe; ¹⁸F-FDG; ¹⁸F-FMISO; ¹⁸F-ML-10; ¹⁸F-Alfatide II; Therapy response; Sunitinib.

Introduction

Angiogenesis is a hallmark of cancer and comprises an essential process to format new blood vessels that supply oxygen and nutrients for cancer growth and development; it is regulated by various independent and interdependent biological factors, including vascular endothelial growth factor (VEGF), extracellular matrix, integrin $\alpha_v\beta_3$ and endothelial cells [1]. Accordingly, antiangiogenesis therapy (AAT) has been developed into biotargeted therapeutic approaches to starve tumors by depriving nutrients and oxygen in clinical settings [2]. For example, several anti-angiogenic drugs, such as bevacizumab, sorafenib and sunitinib, are approved by the FDA to treat human cancers [3]. Although substantial numbers of cancer patients with improved survival have benefitted from ATT in various clinical trials [4-7], some patients do not respond or stop responding over time [8-10]. Therefore, it is urgently necessary to develop highly reliable approaches for the early response monitoring and prediction of AAT efficacy for the optimal management of cancer patients.

Noninvasive medical imaging plays a substantial potential role in monitoring the AAT effects via longitudinally visualizing angiogenesis and the related functional status in preclinical and clinical cancer studies; these imaging tools are important methods for cancer diagnosis and efficacy evaluation in current clinical practices. For example, dynamic contrast-enhanced magnetic resonance imaging (DCE-MRI) and diffusion weighted imaging have been applied to assess tumor blood flow, volume and perfusion to assess the antiangiogenic effect; this MRI approach is comparable to the value of ¹⁸F-fluoro-deoxy-glucose positron emission tomography (¹⁸F-FDG PET) [11, 12]. However, the MRI results for the response assessment to ATT are heterogeneous and sometimes disappointing. Hence, there are substantial challenges for MRI- and CT-based imaging approaches in monitoring the AAT response because they primarily indicate the physical changes of cancer microenvironments related angiogenesis in a qualitative manner rather than a precise and quantitative manner.

In contrast with CT and MRI, PET-based molecular imaging, which comprises the most sensitive imaging modality, holds substantial

advantages for the early response monitoring of AAT because it quantitatively characterizes biological processes at the cellular and molecular levels using bioevent-specific molecular probes [13]. In 2011, Chen and co-colleagues pioneered outstanding studies in this field and published two representative articles almost simultaneously [14, 15]. They reported PET imaging with three ¹⁸F-labeled probes for monitoring the early tumor response to the vascular endothelial growth factor receptor-2 (VEGFR-2) tyrosine kinase inhibitor (TKI) ZD4190, a heteroaromatic anilinoquinazoline analogue, in their initial paper [14]. The authors used ¹⁸F-FDG, 3'-deoxy-3'-¹⁸F-fluorothymidine (¹⁸F-FLT) and ¹⁸F-FPPRGD2, an ¹⁸F-labeled arginine-glycine-aspartic acid (RGD) peptide analog, to assess tumor metabolism, proliferation and angiogenesis, respectively, before and after AAT initiation. In the second paper, they investigated multiplexed PET probes for imaging the early treatment response to VEGF₁₂₁/rGel, a fusion protein that functions as a vascular disruptive agent, in breast cancer models, which included the three previously discussed probes and the fourth probe ¹⁸F-fluoromisonidazole (¹⁸F-FMISO) for imaging tumor hypoxia [15]. These studies demonstrated that imaging proliferation, hypoxia and angiogenesis, rather than imaging metabolism, of cancer may provide highly useful values for the early response evaluation of AAT. It should be noted that the mechanisms of both antiangiogenic drugs against cancer are based on a single-targeted pathway from the view of angiogenesis.

Compared with single-targeted drugs, multi-targeted antiangiogenic drugs are more urgent to perform PET imaging with different probes for monitoring the early response to cancer because targeting several pathways is involved for them to kill cancer by blocking specific receptors or kinases. In 2013, Goggi et al. reported the utility of various PET imaging biomarkers for the early determination of the therapeutic response to the antiangiogenic agent axitinib, a multiple receptor TKI [16]. The authors investigated the imaging of metabolism, proliferation and angiogenesis during the AAT course using ¹⁸F-FDG, ¹⁸F-FLT and ¹⁸F-FtRGD, another RGD peptide analog. Moreover, the immunohistochemical

(IHC) analysis of the microvessel densities (MVD) and Ki-67 was only performed for one time point on day 10 post axitinib treatment; thus, no data were available for the earlier four time points, which were equally important. In our preliminary study in 2014, we demonstrated the values of longitudinal ¹⁸F-FLT PET imaging for monitoring the early response to sunitinib, a multi-targeted TKI, and identified good correlations between the uptake of ¹⁸F-FLT and the scores of Ki-67 and MVD in tumor tissues according to IHC analysis at all imaging time points before and after treatment [17]. A previous study also demonstrated that a ⁶⁴Cu-labeled RGD peptide monomer may provide a sensitive means of monitoring the anti-migratory and anti-proliferative effects of the Src family kinase inhibitor dasatinib [18]. Targets of dasatinib are similar but not identical to sunitinib. Sunitinib mainly targets to VEGFR, PDGFR (platelet-derived growth factor receptor) and c-KIT receptor, and more focuses on antiangiogenic and antitumor effect. It's a worthy question to explore the role of PET imaging in evaluating tumor response to sunitinib. These findings made us confident to further simultaneously investigate the PET molecular imaging of multiple biological parameters, including apoptosis, hypoxia, metabolism and angiogenesis, to monitor and predict the early response and efficacy of multi-targeted AAT in the present study.

Considering the multifactorial complexity and heterogeneity of cancer and especially the ultra-complicated process of cancer responses to therapies, we aimed to profile the biological processes during multi-targeted AAT of sunitinib in U87MG tumor models via PET imaging with four probes, including ¹⁸F-FDG, ¹⁸F-FMISO, ¹⁸F-ML-10 for apoptosis imaging, and ¹⁸F-Alfatide II, a novel ¹⁸F-labeled RGD peptide dimers with easy preparation. Our ultimate goal is to optimize the early response monitoring and prediction of cancer to multi-targeted AAT using noninvasive PET molecular imaging strategies of multifactorial bioparameters.

Materials and Methods

Preparation of ¹⁸F-Labeled PET Probes

¹⁸F-FDG was produced in our PET center and followed the standard protocols used in clinical settings. ¹⁸F-FMISO and ¹⁸F-ML-10 were automatically synthesized using the modified Explora GN module; these procedures have been described in previous publications [19, 20]. ¹⁸F-Alfatide II was prepared in a module-assisted model according to a previously described protocol [21]. Quality controls for each probe were conducted to ensure the quality

requirements of the radiopharmaceuticals prior to use.

Cell Lines and Tumor Models

The human Glioblastoma Multiforme cell line U87MG was obtained from Cell Bank, Shanghai Institutes for Biological Sciences, Chinese Academy of Sciences. The cells were cultured in DMEM medium (Gibco) supplemented with 10% fetal bovine serum and 1% penicillin/streptomycin (P/S) at 37 °C in a humidified atmosphere with 5% CO₂. The cells were subsequently collected via trypsinization with 0.25% trypsin/EDTA. One hundred female athymic Balb/c nude mice (4-6 weeks) were obtained from the Department of Laboratory Animal Science, Fudan University and allowed to acclimate for one week in the animal facility prior to the initiation of the intervention. The U87MG tumor model was generated via a subcutaneous injection of 5.0 × 10⁶ tumor cells in the right shoulder of the mice. Caliper measurements of the perpendicular axes of the tumor were performed to monitor the tumor growth. The mouse weights were also measured. The treatment was initiated when the tumor reached a diameter of approximately 8.0 mm (3 - 4 weeks after inoculation).

Cell Viability Assay

Cell Counting Kit-8 assays (CCK-8, Dojindo Molecular Technologies Inc., San Diego, CA, USA) were performed according to the manufacturer's instructions as an in vitro viability test following the administration of sunitinib. Briefly, 7.0 × 10³ U87MG cells per well (96-well plates) were incubated at 37 °C for 24 h; the cells were subsequently treated with 0.0 nM, 10.0 nM, 100.0 nM, 1.0 μM, 5.0 μM and 10.0 μM of sunitinib (Dalian Melone Pharmaceutical Co., Ltd) in DMEM. At 12 h, days 1, 2, 3, 5 and 7 after therapy initiation, 10.0 μL of CCK-8 were added to each well, followed by incubation for 2 h. The cells were subsequently measured at a wavelength of 450 nm in a Synergy H4 Hybrid Multi-Mode Microplate Reader (BioTek, USA). The absorbance (optical density, OD) at 450 nm was recorded.

Experimental Design *in vivo*

Figure 1 indicates the experimental design used in this study. The mice were randomly assigned to two major groups: the imaging group (*n* = 64) and the immunohistochemistry (IHC) group (*n* = 30). The main purpose of establishing an additional group of mice for the IHC staining was to ensure the accuracy of the IHC data and maintain consistency in the imaging group. Each major group was subsequently divided into the treatment group and the control group. The treatment group was intragastrically administered sunitinib at a dose of 80.0 mg/kg for 7

consecutive days, whereas the control group received an oral administration of vehicle. Sunitinib was suspended in carboxymethylcellulose (CMC) solution (CMC 5%, NaCl 1.8%, Tween 80 0.4%, and benzyl alcohol 0.9% in distilled water) [22]. The mice in the imaging group were imaged via MicroPET/CT with one of the probes (¹⁸F-FDG, ¹⁸F-FMISO, ¹⁸F-ML-10 or ¹⁸F-Alfatide II) on days 0 (before treatment), 1, 3, 7 and 13 following therapy initiation. Tumor samples were collected from the IHC staining group at the corresponding imaging time points for IHC analysis. The tumor dimensions and mouse body weights were measured every other day to monitor the tumor growth. The tumor volume was calculated from the following formula: tumor volume = $a \times (b^2)/2$, where a and b represent the tumor length and width, respectively.

MicroPET/CT Imaging

MicroPET/CT scans and image analysis were performed using an Inveon MicroPET/CT system and the manufacturer-supplied display software (Inveon Research Workplace, Siemens Medical Solution, California, USA). The imaging major group consisted of four subgroups ($n = 16$) of ¹⁸F-FDG, ¹⁸F-FMISO, ¹⁸F-ML-10 and ¹⁸F-Alfatide II, respectively. Each U87MG tumor-bearing mouse in one of the subgroups was injected with 5.55 MBq (150 μ Ci) of the corresponding ¹⁸F-radiolabeled probe via the tail vein. Ten-minute static scans were acquired at 1.0 h post injection, and the animals were maintained under isoflurane anesthesia during the scanning period. The mice in ¹⁸F-FDG group were fasted overnight prior to the probe injection, maintained under isoflurane anesthesia and kept warm during the injection, waiting phase, and scanning periods.

The images were reconstructed using a three-dimensional ordered-subset expectation maximization (OSEM3D)/maximum algorithm. For each MicroPET/CT image, 4.0 mm diameter spherical regions of interest (ROIs) were drawn over both the tumor and the contralateral muscle on the decay-corrected images using Inveon Research Workplace to obtain the percentage of the injected dose per gram (%ID/g). The highest uptake point of the entire tumor was included in the ROI, and no necrosis area was allowed. The ratio of the maximum of the percentage injected dose per gram (%ID/g_{max}) of the tumor to the contralateral muscle (T/M) was calculated.

Immunohistochemistry and Histology

On days 0, 1, 3, 7 and 13 following therapy initiation, to minimize the sampling error of the IHC staining, three sunitinib-treated and three untreated

mice from the IHC group were sacrificed, and tumor samples were collected and fixed in 10% formalin neutral buffer solution for paraffin embedding. The paraffin-embedded tissues were cut into 4- μ m sections and stained with hematoxylin and eosin (H&E) or primary antibody overnight at room temperature; the samples were subsequently visualized with horseradish peroxidase (HRP)-conjugated anti-rabbit/mouse/rat secondary antibodies using an EnViSion Detection Kit (Gene Tech Co. Ltd., Shanghai, China). The following primary antibodies against the different target antigens were used: rabbit anti-human GLUT-1 antibody (1:200, Abcam), rabbit anti-human CA-IX antibody (1:200, Abcam) and rat anti-mouse anti-CD31 (Abcam). After washing with PBS three times for five minutes each time, the immune complexes were visualized using a Peroxidase Substrate DAB Kit (Gene Tech Co. Ltd., Shanghai, China) according to the manufacturer's instructions. Finally, the slices were counterstained with hematoxylin and dehydrated. TUNEL staining was also performed according to the manufacturer's instructions (Roche).

For $\alpha_v\beta_3$ staining, tumor samples were snap-frozen in the OCT (optical cutting temperature) solution and cut into 5- μ m slices. The frozen tumor tissue slices were fixed with ice-cold acetone for 20 min and dried in air for 30 min at room temperature, followed by blocking with 10% normal goat serum for 30 min. The sections were incubated with mouse anti-human integrin $\alpha_v\beta_3$ antibody (1:100, R&D) for 2 h and subsequently visualized with dye-conjugated donkey anti-mouse secondary antibody (1:200, Abcam). After washing 3×5 min with PBS, the whole slices were mounted with 4', 6-diamidino-2-phenylindole (DAPI)-containing mounting medium.

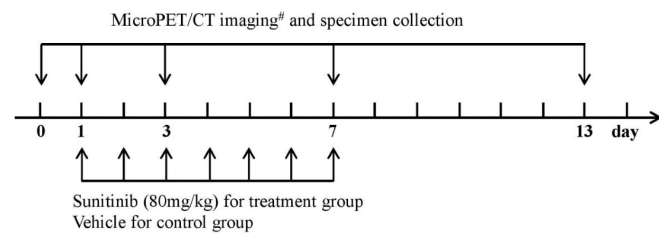


Figure 1: Experimental design for longitudinal MicroPET/CT imaging, tumor sampling and treatment protocols of sunitinib. Notes: # ¹⁸F-FDG, ¹⁸F-FMISO, ¹⁸F-ML-10 and ¹⁸F-Alfatide II were used for MicroPET/CT imaging of U87MG tumor mice.

Immunohistochemistry Analysis

Adobe Photoshop CS5 software and Image-Pro Plus (6.0) software were used to assess the human

Glut-1 intensity, human CA-IX intensity, total TUNEL positive number of nuclei, and human $\alpha_v\beta_3$ fluorescence intensity. The human Glut-1 intensity, human CA-IX intensity, human $\alpha_v\beta_3$ fluorescence intensity and apoptosis index (AI) were calculated by measuring the integrated optical density (IOD) of the images that were of an equivalent area (mm^2). The CD31-positive vessel counting method was modified from the protocol described by Foote et al [23]. The microvessel density (MVD) was assessed using light microscopy in the areas that contained the highest numbers of CD31-positive vessels per area (neovascular "hot spots"). All stained endothelial cells or cell clusters were counted as one microvessel. When two or more positive foci appeared to belong to a single continuous vessel, they were counted as one microvessel. Vessel lumens were not essential. For each tumor section, 3 to 4 random high-powered fields (200 \times) were analyzed.

Statistical Analysis

Quantitative data are presented as means \pm SDs. One-way analysis of variance was used to compare groups of two using SPSS 16.0. Pearson correlation r was performed to calculate the correlations between the probe uptakes from the MicroPET/CT images and immunohistochemistry. P values < 0.05 were considered statistically significant.

Results

Direct Antitumor Effects of Sunitinib on U87MG Tumor Cell Viability in vitro

To determine whether sunitinib induces direct cytostatic or cytotoxic effects in vitro, U87MG cells were treated with sunitinib (0 to 10 μM), and the cell viability was monitored using a CCK-8 assay at different time points post treatment. As shown in **Figure S1**, the low concentrations (10 nM to 1 μM) of sunitinib resulted in little inhibition on cell viability, which increased at the late time points on days 5 and 7 post treatment compared with the control cells. In contrast, sunitinib at the high concentrations of 5 μM to 10 μM resulted in an evident cell inhibitory capability as early as days 1 and 2 post treatment, which significantly delayed and, in some cases, stopped the growth of U87MG cells. Therefore, sunitinib treatment led to an inhibitory effect on U87MG cell viability in a dose- and time-dependent manner at specific concentrations.

Significant Delay Effects of Sunitinib on U87MG Tumor Growth

As expected, 7 consecutive administrations of sunitinib at the daily dose of 80 mg/kg produced a

significant delay in the tumor volume. According to **Figure 2A**, a time-related increase in the tumor size was identified in the control group, in which the average percentages of the tumor volume increase, expressed as $(V-V_0)/V_0$, were 9.3 ± 8.2 , 49.2 ± 27.7 , 269.8 ± 56.9 and $876.3 \pm 240.1\%$ on days 1, 3, 7 and 13, respectively. As a comparison, sunitinib treatment resulted in a reduced tumor size increase, which was 6.7 ± 8.5 , 22.0 ± 21.4 , 75.0 ± 52.6 and $616.9 \pm 119.3\%$ on days 1, 3, 7 and 13, respectively. There was a significant difference in the tumor size between the sunitinib and control groups after day 9 ($P < 0.01$). Moreover, as shown in **Figure 2B**, no significant loss of body weight was identified during the sunitinib treatment period at the dosage of 80 mg/kg used in this study. This finding indicated that sunitinib has no obvious toxic side effects using the prescribed protocol.

Increased Glucose Metabolism of U87MG Tumors in the Late Stage of Sunitinib Treatment

^{18}F -FDG PET/CT imaging is routinely applied to quantitatively measure the glucose metabolism of tumors *in vivo* both in preclinical and clinical settings. In the current study, static ^{18}F -FDG MicroPET/CT scans at 1.0 h post injection were acquired on days 0 (baseline), 1, 3, 7 and 13. The representative images are shown in **Figure 3A**, and the quantitative %ID/ g_{\max} and T/M values of the tumor uptake of ^{18}F -FDG are presented in **Figures 3B** and **3C**. For the sunitinib group, the tumor uptake values %ID/ g_{\max} of ^{18}F -FDG were 9.5 ± 2.3 , 9.3 ± 2.0 , 12.3 ± 1.8 , 13.8 ± 3.4 and 17.2 ± 2.8 on days 0, 1, 3, 7 and 13, respectively. These results exhibited an increase trend, and a significant difference was identified from day 7 ($P < 0.01$) during the late phase compared with the baseline level. In contrast, the %ID/ g_{\max} in the control group remained a stable area of approximately 12.1 throughout the two-week study, and no significant difference was identified.

To verify the relationship between ^{18}F -FDG uptake and Glut-1 expression, immunohistochemistry staining of Glut-1 was assessed. As shown in **Figures 3D** and **3E**, the Glut-1 intensity in the sunitinib group was increased compared with the control group, which was consistent with the results demonstrated by ^{18}F -FDG PET/CT imaging. However, there was no significant difference in the Glut-1 expression between or within both groups. Moreover, only a weakly positive correlation between the ^{18}F -FDG uptake and Glut-1 intensity was identified with no significant difference ($r = 0.309$, $P = 0.385$, **Figure 3F**).

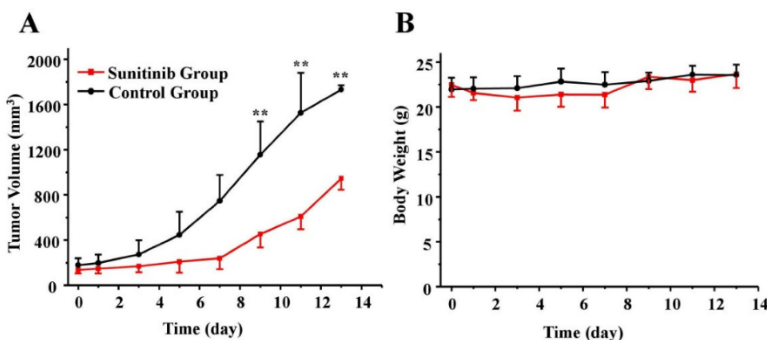


Figure 2: Effects of sunitinib on antitumor activity (A) and body weight (B) in U87MG tumor mice over time. U87MG tumor-bearing mice were treated with sunitinib or vehicle. There was significant difference for the tumor size between the sunitinib group and control group post day 9 ($P < 0.01$). On the other hand, there was no difference for the mice weight between the sunitinib group and control group. ** $P < 0.01$.

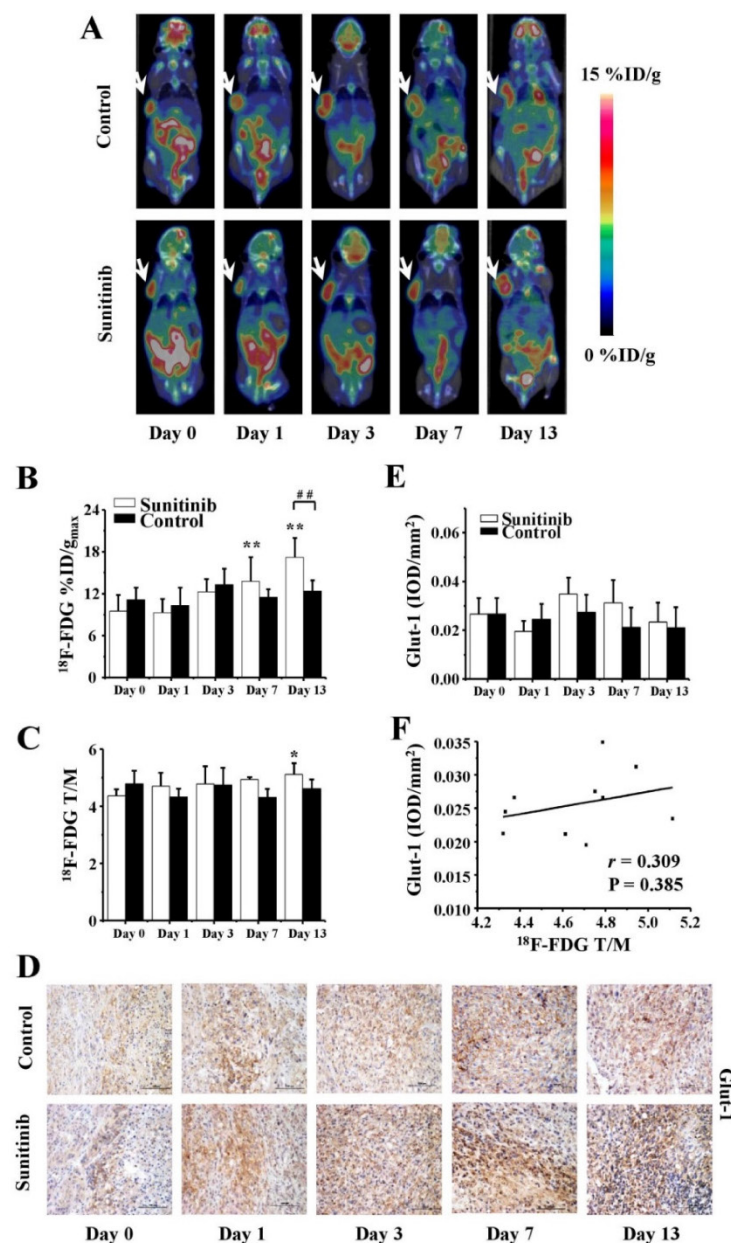


Figure 3: ¹⁸F-FDG MicroPET/CT imaging of U87MG tumor-bearing mice, IHC staining for Glut-1 of tumor tissues and the relevant quantitative and correlation analysis. (A) Representative MicroPET/CT images at 1.0 h after intravenous injection of ¹⁸F-FDG (5.55 MBq per mouse) on days 0, 1, 3, 7 and 13 post treatment. (B, C) Quantitative %ID/g_{max} of tumor uptake and the ratios of tumor to contralateral muscle (T/M) in the sunitinib and control groups based on ROIs analysis from ¹⁸F-FDG MicroPET/CT. (D, E) IHC and quantitative analysis of tumor sections about Glut-1. (F) Correlations between ¹⁸F-FDG T/M and Glut-1 expression of tumor. Notes: The tumors were indicated by arrows. * $P < 0.05$, ** $P < 0.01$, within the sunitinib group, compared to day 0. # # $P < 0.01$, between the sunitinib group and the control group.

Reduced Tumor Hypoxia in the Early Stage of Sunitinib Treatment

To assess the tumor hypoxia changes induced by sunitinib, longitudinal ^{18}F -FMISO MicroPET/CT imaging was performed at the same time points as ^{18}F -FDG. Typical images and the quantitative data ($\% \text{ID}/\text{g}_{\max}$ and T/M) are presented in **Figures 4A-C**. For the sunitinib group, the tumor uptake of ^{18}F -FMISO was significantly decreased on days 1 and 3 after treatment ($T/M_0 = 2.04 \pm 0.18$, $T/M_3 = 1.57 \pm 0.12$, $P < 0.01$) compared with the baseline level. This finding indicated that sunitinib reduced the tumor hypoxia level during the early stage. However, the uptake of ^{18}F -FMISO was restored close to baseline on days 7 and 13, which implied that sunitinib slightly induced tumor hypoxia during the late stage. As a

comparison, ^{18}F -FMISO uptake in the control group continued to stably increase throughout the 13-day period. It was notable that both the $\% \text{ID}/\text{g}_{\max}$ and T/M of the ^{18}F -FMISO uptake in the sunitinib group were lower compared with the control group, which indicated that sunitinib lessened the hypoxia degree of the tumor microenvironment in general.

Consistent with the ^{18}F -FMISO PET imaging of tumor hypoxia, the expression level of CA-IX, a promising endogenous hypoxia-related cell surface enzyme, also exhibited similar change trends in both the treatment and control groups (**Figures 4D and 4E**). Furthermore, there was a significantly positive correlation between the ^{18}F -FMISO uptake and the CA-IX intensity ($r = 0.962$, $P < 0.001$, **Figure 4F**).

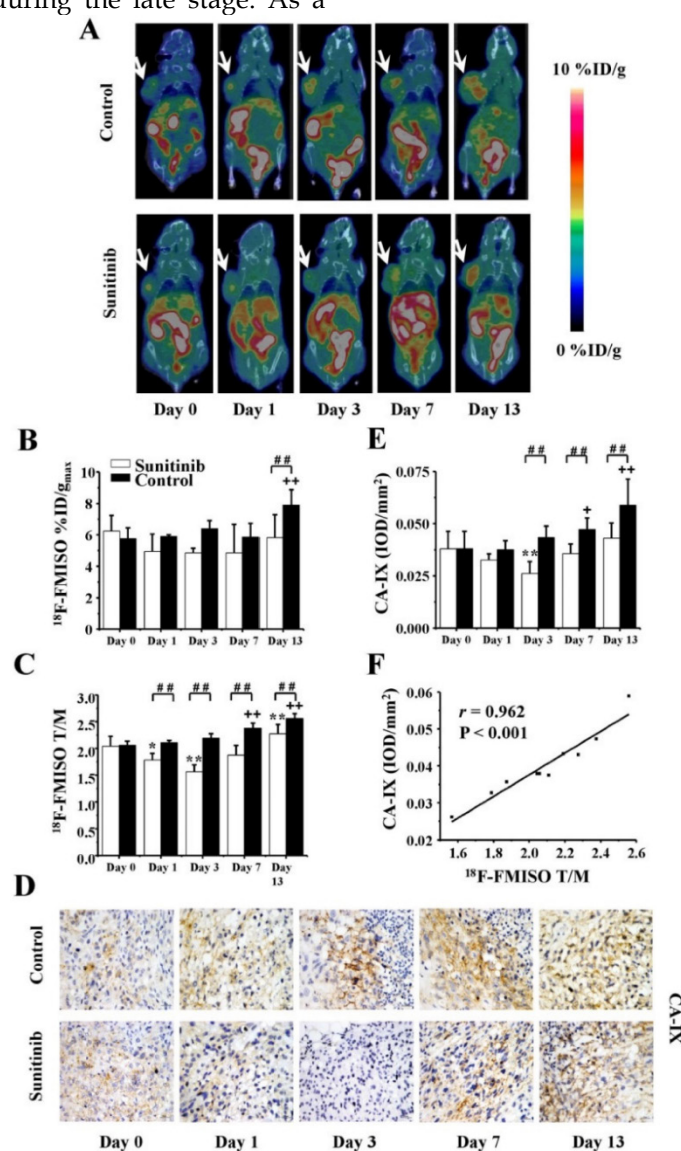


Figure 4: ^{18}F -FMISO MicroPET/CT imaging of U87MG tumor-bearing mice, IHC staining for CA-IX of tumor tissues and the relevant quantitative and correlation analysis. (A) Representative MicroPET/CT images at 1.0 h after intravenous injection of ^{18}F -FMISO (5.55 MBq per mouse) on days 0, 1, 3, 7 and 13 post treatment. (B, C) Quantitative $\% \text{ID}/\text{g}_{\max}$ of tumor uptake and the ratios of tumor to contralateral muscle (T/M) in the sunitinib and control groups based on ROIs analysis from ^{18}F -FMISO MicroPET/CT. (D, E) IHC and quantitative analysis of tumor sections about CA-IX. (F) Correlations between ^{18}F -FMISO T/M and CA-IX expression of tumor. Notes: The tumors were indicated by arrows. * $P < 0.05$, ** $P < 0.01$, within the sunitinib group, compared to day 0. + $P < 0.05$, ++ $P < 0.01$, within the control group, compared to day 0. # $P < 0.01$, between the sunitinib group and the control group.

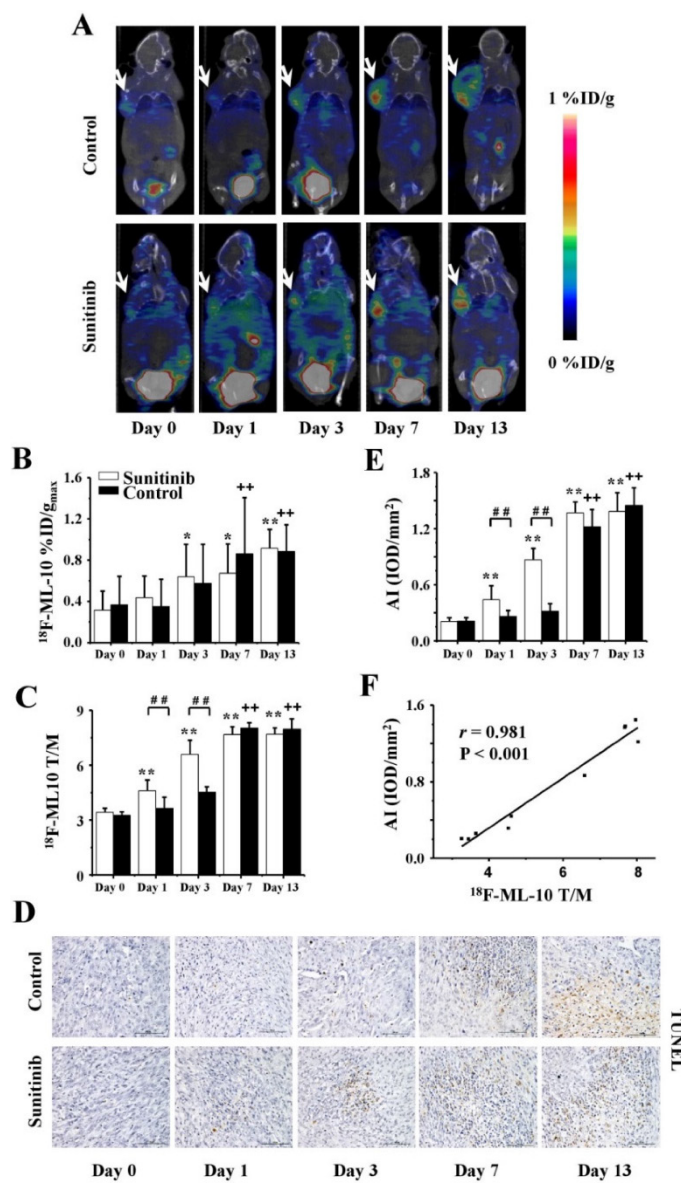


Figure 5: ^{18}F -ML-10 MicroPET/CT imaging of U87MG tumor-bearing mice, IHC staining for TUNEL of tumor tissues and the relevant quantitative and correlation analysis. (A) Representative MicroPET/CT images at 1.0 h after intravenous injection of ^{18}F -ML-10 (5.55 MBq per mouse) on days 0, 1, 3, 7 and 13 post treatment. (B, C) Quantitative $\% \text{ID}/\text{g}_{\max}$ of tumor uptake and the ratios of tumor to contralateral muscle (T/M) in the sunitinib and control groups based on ROIs analysis from ^{18}F -ML-10 MicroPET/CT. (D, E) IHC and quantitative analysis of tumor sections about TUNEL. (F) Correlations between ^{18}F -ML-10 T/M and AI from TUNEL. Notes: The tumors were indicated by arrows. * $P < 0.05$, ** $P < 0.01$, within the sunitinib group, compared to day 0. + + $P < 0.01$, within the control group, compared to day 0. # # $P < 0.01$, between the sunitinib group and the control group.

Increased Tumor Apoptosis in the Early Stage of Sunitinib Treatment

To identify tumor apoptosis mediated by sunitinib, serial ^{18}F -ML-10 MicroPET/CT imaging was performed at the corresponding time points previously described. The high quality of the images with the full data of the $\% \text{ID}/\text{g}_{\max}$ and T/M are displayed in Figures 5A-C. On days 1 and 3, the tumor uptakes of ^{18}F -ML-10 in the sunitinib group substantially increased compared with the control group, and significant differences for the T/M between both groups were also identified ($P < 0.01$).

These findings suggested that sunitinib increased U87MG tumor apoptosis during the early stage. However, there was no significant difference in the ^{18}F -ML-10 uptake between the two groups on days 7 and 13 ($P > 0.05$). In general, the tumor uptake of ^{18}F -ML-10 in both groups continuously increased from days 1 through 13.

Consistent with the ^{18}F -ML-10 uptake from the PET imaging of tumor apoptosis, a TUNEL assay indicated that the apoptotic index (AI) in both the treatment and control groups exhibited similar increase trends (Figures 5D and 5E). Moreover, a

significantly positive correlation between the ^{18}F -ML-10 uptake and the TUNEL-based AI was also identified ($r = 0.981$, $P < 0.001$, Figure 5F).

Decreased Tumor Angiogenesis following Sunitinib Treatment

To measure the effects of sunitinib on U87MG tumor angiogenesis, ^{18}F -Alfatide II MicroPET/CT imaging was longitudinally performed on days 0 (baseline), 1, 3, 7 and 13. Clear PET images in combination with the quantitative data of the %ID/g_{max} and T/M are shown in Figures 6A-C. For the sunitinib group, the tumor uptake of ^{18}F -Alfatide II substantially decreased during the consecutive 7-day therapy and reached the lowest value on day 7.

For example, the T/M values were as follows: $\text{T}/\text{M}_0 = 5.3 \pm 0.2$, $\text{T}/\text{M}_1 = 4.6 \pm 0.3$, $\text{T}/\text{M}_3 = 3.8 \pm 0.1$ and $\text{T}/\text{M}_7 = 3.1 \pm 0.1$, where all $P < 0.01$ (compared with T/M_0). On day 13, six days after the treatment withdrawal, the ^{18}F -Alfatide II uptake had recovered; however, it remained significantly decreased compared with the baseline level ($\text{T}/\text{M}_{13} = 4.3 \pm 0.2$, $P < 0.01$). On the contrary, the ^{18}F -Alfatide II uptake in the control group remained relatively stable from days 0 to 13. Moreover, significant differences were also identified for the ^{18}F -Alfatide II uptake between the sunitinib and control groups on days 1, 3, 7 and 13, where all P values were less than 0.01.

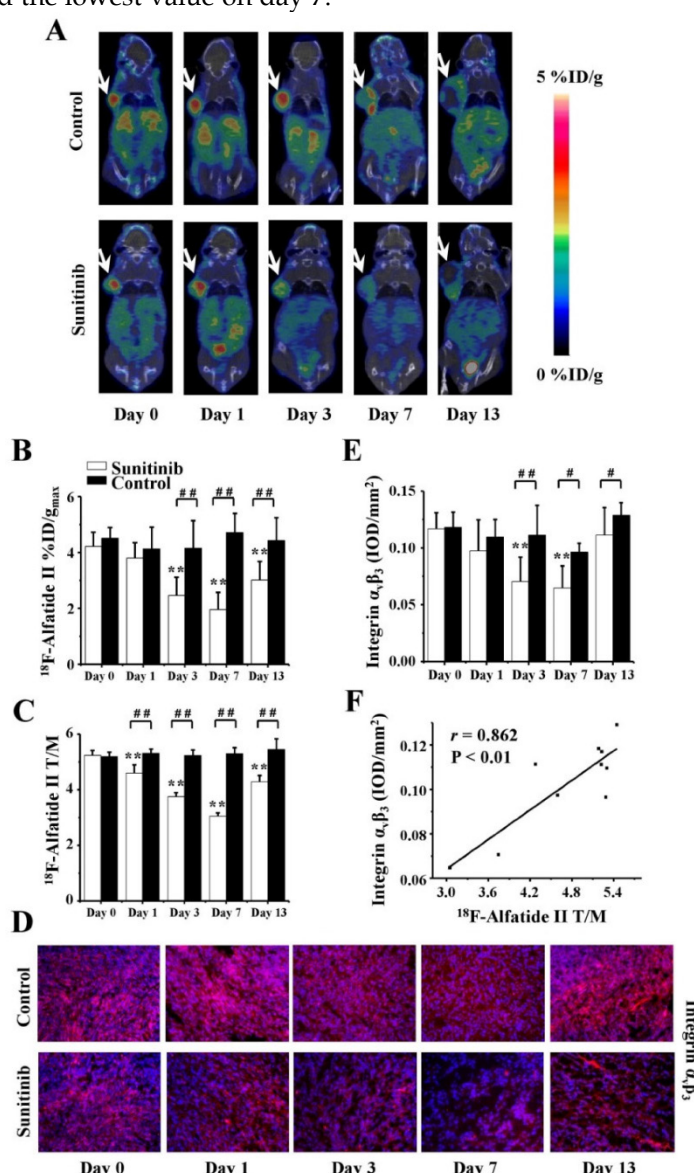


Figure 6: ^{18}F -Alfatide II MicroPET/CT imaging of U87MG tumor-bearing mice, IHC staining for integrin $\alpha_1\beta_3$ of tumor tissues and the relevant quantitative and correlation analysis. (A) Representative MicroPET/CT images at 1.0 h after intravenous injection of ^{18}F -Alfatide II (5.55 MBq per mouse) on days 0, 1, 3, 7 and 13 post treatment. (B, C) Quantitative %ID/g_{max} of tumor uptake and the ratios of tumor to contralateral muscle (T/M) in the sunitinib and control groups based on ROIs analysis from ^{18}F -Alfatide II MicroPET/CT. (D, E) IHC and quantitative analysis of tumor sections about integrin $\alpha_1\beta_3$. (F) Correlations between ^{18}F -Alfatide II T/M and integrin $\alpha_1\beta_3$ expression of tumor. Notes: The tumors were indicated by arrows. ** $P < 0.01$, within the sunitinib group, compared to day 0. # $P < 0.05$, ## $P < 0.01$, between the sunitinib group and the control group.

Consistent with the ^{18}F -Alfatide II PET imaging of tumor angiogenesis, the expression level of integrin $\alpha_v\beta_3$ exhibited a similar alteration tendency (**Figures 6D and 6E**). The fluorescence intensity of $\alpha_v\beta_3$ was approximately 0.12 prior to therapy and then significantly decreased to 0.07 ± 0.02 on day 3 ($P < 0.01$) and 0.06 ± 0.02 on day 7 ($P < 0.01$) after sunitinib treatment; it returned to baseline on day 13 (after drug withdraw). The quantitative data regarding the integrin $\alpha_v\beta_3$ intensity and ^{18}F -Alfatide II uptake were also positively correlated ($r = 0.862$, $P < 0.01$, **Figure 6F**).

As the reference criterion of anti-angiogenic activity, the MVD was further assessed via IHC staining of CD31. As shown in **Figure 7A**, CD31-positive staining was broadly identified in the tumor sections in the control group, which indicated a relatively abundant MVD. Following sunitinib treatment, the MVD level substantially decreased in the tumor slices as a result of the effective anti-angiogenic activity of sunitinib. For example, the MVD level decreased to 36.33 ± 3.64 on day 1 after therapy compared with the control group (61.88 ± 0.16 , $P = 0.003$) and continuously decreased until day 7 ($P < 0.01$). These findings indicated that sunitinib

induced effective anti-angiogenic activity against solid cancers, such as U87MG tumor xenografts.

Correlations between MVD and Metabolism, Hypoxia, Apoptosis and Angiogenesis of Tumors

Tumor blood vessels constitute the network basis of the microenvironment functions; thus, the microvessel densities should have an extensive influence on the metabolism, hypoxia, apoptosis and angiogenesis of tumors. To further validate the feasibility of monitoring the early response to AAT, the correlations between the MVD and the tumor uptakes of the four ^{18}F -labeled probes were investigated. As expected, a strongly positive correlation was identified between the ^{18}F -Alfatide II uptake and the MVD ($r = 0.954$, $P < 0.001$). Interestingly, there were also weakly negative or positive correlations between the MVD and the uptakes of ^{18}F -FDG ($r = -0.611$), ^{18}F -FMISO ($r = 0.564$) and ^{18}F -ML-10 ($r = -0.556$); however, these correlations were not statistically significant (all $P > 0.05$) (**Figures 7B-E**). H&E staining of the tumor sections was also performed on days 0, 1, 3, 7 and 13 after treatment was initiated (**Figure S2**).

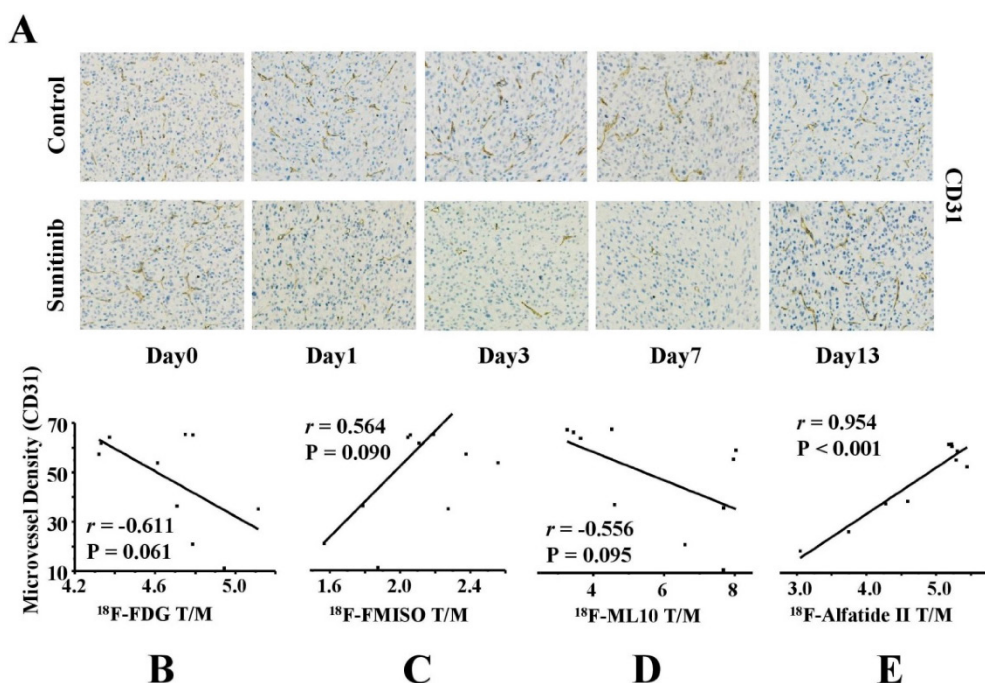


Figure 7: IHC analysis of tumor sections about CD31 on days 0, 1, 3, 7 and 13 post therapy and the correlations with T/M of each probe. (A) Representative captures of CD31 staining of tumor tissues in sunitinib and control groups (40×10). CD31 in the sunitinib group revealed effective antiangiogenic activity from days 1 to 7. MVD in sunitinib group lowered significantly than that in control group. (B-E) Correlations between MVD and T/M of each probe (^{18}F -FDG, ^{18}F -FMISO, ^{18}F -ML-10, ^{18}F -Alfatide II, from Left to Right).

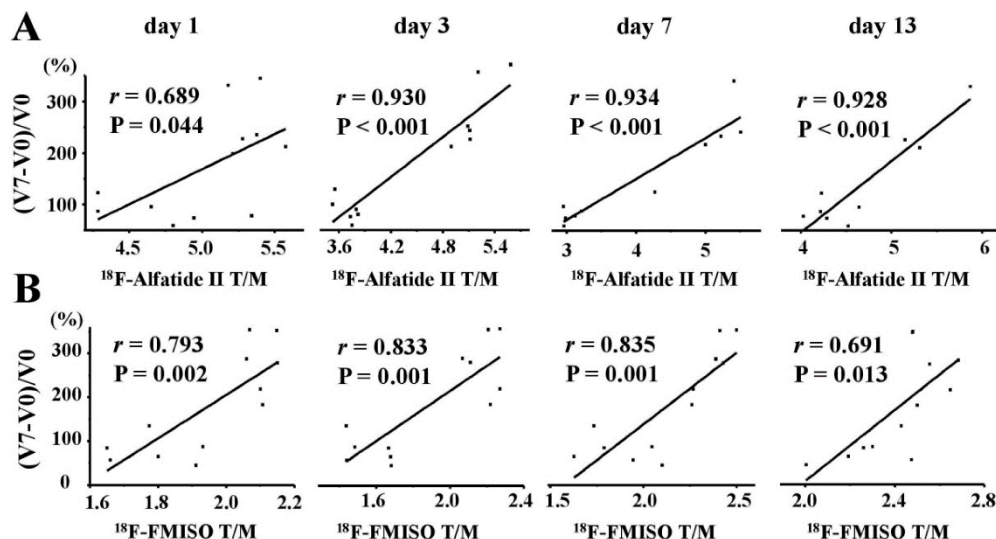


Figure 8: Correlations between tumor growth ratios (TGR) and T/M of ^{18}F -Alfatide II (A) and ^{18}F -FMISO (B) on days 1, 3, 7 and 13 (from Left to Right). There were significantly positive correlations between the TGR and the T/M of ^{18}F -Alfatide II and ^{18}F -FMISO.

Efficacy Prediction of Sunitinib to U87MG Tumors via PET Molecular Imaging of Hypoxia and Angiogenesis

To predict the AAT efficacy using noninvasive PET molecular imaging of multifactorial bioparameters, we further explored the correlations between the tumor growth ratios (TGR) at the end of treatment and the T/M of the PET probes. Day 7 was the end time of the whole ATT protocol, so TGR on day 7 was selected to verify the objective effectiveness of sunitinib and observe cancer biology during ATT. The TGR was expressed as the ratio of $(V_7 - V_0) / V_0$, where V_0 and V_7 represented the tumor volumes on days 0 and 7, respectively. There were significantly positive correlations between the TGR and the T/M of ^{18}F -Alfatide II (Figure 8A) on days 1 ($r = 0.689$, $P = 0.044$), 3 ($r = 0.930$, $P < 0.001$), 7 ($r = 0.934$, $P < 0.001$) and 13 ($r = 0.928$, $P < 0.001$). Surprisingly for ^{18}F -FMISO (Figure 8B), positively good correlations between the TGR and the T/M were also identified on days 1 ($r = 0.793$, $P = 0.002$), 3 ($r = 0.833$, $P = 0.001$), 7 ($r = 0.835$, $P = 0.001$) and 13 ($r = 0.691$, $P = 0.013$). However, no significant correlations between the TGR and the T/M of ^{18}F -FDG and ^{18}F -ML-10 were identified (Figure S3).

Discussion

Cancer antiangiogenesis therapy, especially for multi-targeted drugs, induces complex biochemical events, such as the up-regulation of anti-angiogenic, pro-apoptotic and hypoxic-related factors, which eventually influence the angiogenesis, apoptosis/proliferation, hypoxia and metabolism of tumor cells. Therefore, to optimize the early response

monitoring and prediction of cancer AAT in this study, we performed longitudinal, noninvasive PET molecular imaging with different ^{18}F -labeled probes in U87MG tumor xenografts treated with the multi-targeted TKI sunitinib. The experimental design is shown in Figure 1. To comprehensively characterize the biochemical processes and microenvironmental status, four molecular probes, including ^{18}F -FDG, ^{18}F -FMISO, ^{18}F -ML-10 and ^{18}F -Alfatide II, were used to image the energy (glucose) metabolism, tumor hypoxia, cell apoptosis and angiogenesis, respectively, via serial MicroPET/CT scans before and after sunitinib treatment. It was notable that each probe was assigned an individual group of U87MG tumor mice for the corresponding PET scanning, which enabled exact imaging time points. That is, it avoided imaging at earlier or later time points, which occurred when one group of mice were used for all probes in previous publications. Moreover, a dedicated group of mice were used to collect tumor tissues at the corresponding time points for IHC staining. This approach ensured the accuracy of the IHC data because there was no influence of injection and imaging on the tumor, and it also maintained the consistency of the mouse number in the imaging group. This type of reasonable design was vital to the experimental results and conclusions; however, it's an unavoidable challenge to get involved with inter-subject variation, so the best efforts were made to minimize the controllable influence factors, such as enlarging sample size, stabilizing mouse source and feeding environment, as well as gently handling model mice. In our previous study [17], we compared 5 parameters: SUV_{mean} , SUV_{max} , $\% \text{ID}_{\text{gmean}}$, $\% \text{ID}_{\text{gmax}}$

and T/M of %ID/g_{max}, as a result, we found that only T/M of %ID/g_{max} showed statistical value. That is why T/M of %ID/g_{max} was used as the main parameter in this study.

¹⁸F-FDG PET/CT has been routinely used for cancer diagnosis and efficacy evaluation via quantitative determinations of glucose metabolism in vivo in clinical and preclinical settings. In general, effective therapy often results in a decrease in ¹⁸F-FDG uptake in disease lesions. However, our results demonstrated the ¹⁸F-FDG uptakes in the U87MG tumor lesions significantly increased during the late stage of sunitinib treatment (Figure 3), which was consistent with the Glut-1 expression of tumor tissues ex vivo. Nevertheless, sunitinib exhibited evident anti-tumor effects in vitro and in vivo (Figure S1, Figure 2A). These findings appear to differ from the conventional opinions regarding the effects of anti-cancer drugs on glucose metabolism of tumors. For example, previous studies have reported no significant change in the ¹⁸F-FDG uptake in MDA-MB-435 tumors after treatment with ZD4190 or VEGF₁₂₁/rGel [14, 15]. Goggi et al. reported a substantial decrease in ¹⁸F-FDG uptake in U87MG and MDA-MB-231 tumors on day 10 after axitinib treatment [16]. These findings appear contradictory regarding the effects of anti-angiogenic drugs on glucose uptake of tumors. We speculated that each anti-angiogenic drug may have different influences on the glucose transporter in different tumor models.

Hypoxia, which represents an insufficient oxygen concentration in tissues far from the blood supply, is an intrinsic component of solid cancers. ¹⁸F-FMISO PET/CT imaging may be used to quantitatively map the hypoxic degree in various types of cancers with high sensitivity [24]. In this study, we performed ¹⁸F-FMISO MicroPET/CT imaging at 1.0 h p.i., because time points less than 2.0 h, like 1.5 h p.i., were often used in preclinical studies [25, 26]. Moreover, our group demonstrated that T/M was one of the important parameters for ¹⁸F-FMISO PET, and the cutoff value of >1.2 can predict primary endocrine resistance in clinical study [27]. Since almost all the T/M ratios were more than 1.5 and ¹⁸F-FMISO PET imaging had good contrast in this study, 1.0 h p.i. as imaging time point was relatively feasible. According to the PET images and ¹⁸F-FMISO uptake data, we identified a transient decrease in the ¹⁸F-FMISO uptake in the sunitinib-treated tumors on days 1 and 3 after therapy, followed by a continuous increase from days 7 to 13. The hypoxic trends were further assessed via ex vivo IHC staining of CA-IX, a hypoxia marker. The results indicated that anti-angiogenic drugs, such as sunitinib, reduced U87Mg tumor hypoxia during the early stage. There

are two possible reasons for this phenomenon: the broken vascular reduced perfusion and therefore the delivery of ¹⁸F-FMISO was excluded, since ¹⁸F-FMISO uptake from days 3 to 7 were increased rather than decreased. Another acknowledged explanation for this phenomenon may be that anti-angiogenic agents transiently “normalize” the tumor vasculature to temporally improve the oxygen supply of the tumor blood flow [28]. These phenotypic changes in the vasculature may reflect the balance of pro- and anti-angiogenic factors in the tumor [29]. Hypoxia may induce resistance to chemotherapy and radiotherapy; thus, combined therapies with AAT at the window of reduced hypoxia, such as from days 1 to 3 after sunitinib treatment in this study, would produce a maximum curative effect. Therefore, sequential ¹⁸F-FMISO PET/CT scans may be necessary for AAT-based combination therapies because this approach may be used to identify the optimal window of “vascular normalization” as a result of AAT effects.

The anti-tumor effects of AAT have been attributed, in part, to the ability to induce cell apoptosis because multi-targeted anti-angiogenic drugs, such as sunitinib, exhibit a pro-apoptotic capability to arrest tumor growth. Thus, we performed serial ¹⁸F-ML-10 MicroPET/CT to determine the apoptosis level induced by AAT. ¹⁸F-ML-10 is a newly-emerged small molecule probe for apoptosis imaging, which selectively targets apoptotic cells rather than necrotic cells [30]. The ¹⁸F-ML-10 data indicated increased apoptosis of U87MG tumors induced by sunitinib during the early stage, which was significantly increased compared with the control group. The tumor apoptosis was fully confirmed via TUNEL assay. Since spontaneous apoptosis is one of the inherent features of cancer cells, we speculated that the jump increases of ¹⁸F-ML-10 uptake and apoptotic index (TUNEL) between days 3 and 7 in control group was due to the spontaneous apoptosis during the 4-day period. As contrast, the tumor size in the therapy group increased gradually, and both T/M of ¹⁸F-ML-10 and TUNEL staining presented a relatively gentle increase. ¹⁸F-ML-10 exhibited a high and stable tumor-to-blood ratio from 30 min after probe administration because of the rapid clearance from non-target organs and blood circulation in the first human study [31]. Oborski et al. subsequently reported the successful use of ¹⁸F-ML-10 PET for the early response assessment of radiotherapy in glioblastoma multiforme patients [32]. In addition to ¹⁸F-ML-10, the radionuclides ^{99m}Tc- and ¹⁸F-labeled Annexins play important roles in apoptosis imaging [33, 34]. However, these Annexin-based probes have

been associated with substantial challenges in monitoring the therapy efficacy, such as AAT, in clinical trials. One potential reason is that the damaged blood vessels impair the delivery of Annexins, which comprise macromolecular proteins with high molecular weights, to tumor tissue [35]. Our findings demonstrate the substantial potential value of ¹⁸F-ML-10 PET/CT imaging for monitoring the early response of sunitinib and measuring changes in cell apoptosis during AAT.

We have previously investigated the value of quantitative ¹⁸F-FLT MicroPET/CT imaging for monitoring cell proliferation and the early response to sunitinib in U87MG tumor xenografts because proliferation, in contrast to apoptosis, is a vital aspect of cell fate [17]. ¹⁸F-FLT imaging indicated a decrease in tumor cell proliferation from day 1 after sunitinib therapy, which was confirmed by Ki67 staining. Other clinical and preclinical studies have also indicated that ¹⁸F-FLT uptake rapidly decreased in response to radiotherapy, cytotoxic chemotherapy and cytostatic AAT [14, 36-39].

The ability to inhibit tumor angiogenesis primarily accounts for the anti-cancer effects of AAT. The integrin $\alpha_v\beta_3$ receptor is overexpressed on tumor neovasculatures, and it binds to RGD peptides with high affinity. Therefore, several ¹⁸F-radiolabeled RGD analogs, such as ¹⁸F-FPPRGD2, have been developed as PET molecular imaging probes to visualize the $\alpha_v\beta_3$ expression and evaluate the response of AAT in preclinical studies or clinical trials [16, 21, 40]. In a previous study, 60 mg/kg of sunitinib induced a decrease in ¹⁸F-Fuciclatide uptake in U87MG tumor sites from day 2, and a significantly decreased MVD level was identified on day 13 compared with the control animals [41]. However, ¹⁸F-Fluciclatide need a complicated, multi-step synthesis procedure; moreover, the previous MVD analysis lacked histopathological data from tumor samples at early time points to enable a longitudinal comparison. Furthermore, the multi-step, time-consuming preparation may hamper the clinic translation in the future. Recently, ¹⁸F-Alfatide, which has a simple preparation and short synthesis time, was developed using the facile chelate method via Al-¹⁸F [42]. Clinical studies of ¹⁸F-Alfatide have successfully been conducted with promising results [43]. In the present study, we employed ¹⁸F-Alfatide II MicroPET/CT imaging to monitor the U87MG response to sunitinib. The imaging data indicated a decreased tumor uptake of ¹⁸F-Alfatide II as a result of the reduced tumor angiogenesis from days 1 to 13 in the sunitinib group. These findings were consistent with the results of IHC staining of $\alpha_v\beta_3$ and CD31. It should be noted that only the human integrin $\alpha_v\beta_3$ on U87MG tumor cells

was assessed via IHC staining using anti-human integrin $\alpha_v\beta_3$ antibody, whereas the murine integrin $\alpha_v\beta_3$ on tumor vascular endothelial cells was not assessed using anti-mouse integrin β_3 , which was a limitation of this study. Using an alternative, indirect way, we performed IHC staining of anti-mouse CD31 antibody to measure tumor MVD, since vascular endothelial cells, expressing murine integrin $\alpha_v\beta_3$, are the major component of tumor neovasculature. The similar MVD protocol was reported to evaluate angiogenesis change and MVD level correlated with the uptake of radiolabeled RGD peptides in literatures with comprehensive discussions [18, 41]. Moreover, U87MG xenograft models have been well-documented to express integrin $\alpha_v\beta_3$ on both tumor cells and neovasculatures, and the tumor uptake of ^{99m}Tc-labeled RGD probe was correlated with two-origin integrin $\alpha_v\beta_3$ reported by Liu et al. [44]. Although our results were in line with those in previous studies about monitoring AAT response using RGD-based imaging, measurement of murine integrin $\alpha_v\beta_3$ is planning in our following studies, which should be strongly recommended for this type of investigations.

In a new study, Gao et al. reported that the Src inhibitor dasatinib reduced the uptake of ^{99m}Tc-3PRGD2 in a dasatinib-resistant A549 human non-small cell lung cancer model [45]. They attributed this effect to the down-regulation of the host (murine) integrin β_3 and the reduced RGD binding affinity for tumor (human) integrin $\alpha_v\beta_3$ because the expression of the tumor (human) integrin $\alpha_v\beta_3$ did not change according to the IHC assays. It was reported dasatinib treatment substantially changed the cell surface distribution of the integrin $\alpha_v\beta_3$ [18]. It appears that anti-angiogenesis drugs with different mechanisms may induce integrin in different statuses. Therefore, additional studies are necessary to investigate the interrelations between the uptake of RGD-based tracers and the integrins from host-guest origins following anti-cancer drug treatments, such as AAT. Furthermore, another question was raised for those two reports [18, 45] whether RGD peptides alone could be sufficient enough to reflect tumor response to dasatinib therapy since dasatinib treatment lead to the uptake reduction of the radiolabeled RGD in both dasatinib-responsive U87MG tumor and dasatinib-resistant A549-fLuc tumor model. To strengthen the current study, a sunitinib-resistant tumor model is really necessary. Alternatively, untreated U87MG tumors were used as control, which was also a limitation of this study. As one of this series of research, the related project using sunitinib-resistant tumor model is under considerations.

Overall, we evaluated the sunitinib therapy response in U87MG xenografts from four aspects of tumor biology using longitudinal MicroPET/CT imaging, including glucose metabolism (¹⁸F-FDG), hypoxia (¹⁸F-FMISO), apoptosis (¹⁸F-ML-10) and angiogenesis (¹⁸F-Alfatide II). The uptakes of ¹⁸F-FMISO, ¹⁸F-ML-10 and ¹⁸F-Alfatide II in the tumor lesions significantly changed during the early stage (days 1 to 3) of sunitinib treatment, whereas the ¹⁸F-FDG uptake was altered during the late stage. The PET imaging of ¹⁸F-FDG was less sensitive compared with the other three probes for monitoring the early cancer response to the anti-angiogenic drug sunitinib in U87MG tumors. From a conventional view of the histopathology criterion, the MVD significantly correlated with the PET imaging of ¹⁸F-Alfatide II; however, the correlation was not significant for the other three probes. This finding was reasonable because of the direct or indirect relationships with the MVD. For the end evaluation criterion of the therapeutic efficacy, PET imaging of ¹⁸F-Alfatide II and ¹⁸F-FMISO was significantly correlated with the TGR, whereas the imaging of ¹⁸F-FDG and ¹⁸F-ML-10 was not significantly correlated with the TGR. To the best of our knowledge, this finding has not been reported in the published literature. Based on the tumor uptake of the PET probes and their correlations with the MVD and TGR, ¹⁸F-Alfatide II PET imaging was sensitive to optimize early AAT response monitoring and feasible to precisely predict the AAT efficacy, such as sunitinib, in U87MG tumors.

Conclusion

Using PET imaging, we applied four types of specific molecular probes, including ¹⁸F-FDG (metabolism), ¹⁸F-FMISO (hypoxia), ¹⁸F-ML-10 (apoptosis) and ¹⁸F-Alfatide II (angiogenesis), to quantitatively assess the vital biological and microenvironmental changes of U87MG tumors treated with the anti-angiogenic drug sunitinib. In conclusion, it is feasible to optimize the early response monitoring and precise efficacy prediction of cancer anti-angiogenesis therapy using the noninvasive PET molecular imaging strategy of ¹⁸F-Alfatide II. These preclinical findings will provide valuable benefits for the response monitoring, outcome prediction and treatment planning of AAT and related combination therapies using PET molecular imaging of tumor biology, such as angiogenesis imaging with ¹⁸F-Alfatide II, which represents an RGD-based probe.

Supplementary Material

Supplementary figures.

<http://www.thno.org/v06p2084s1.pdf>

Acknowledgements

This study was partly supported by National Natural Science Foundation of China (No. 11275050, No. 30700188). We are greatly thankful to Prof. Xiaoyuan Chen and Dr. Lixin Lang from the Laboratory of Molecular Imaging and Nanomedicine, National Institute of Biomedical Imaging and Bioengineering, National Institutes of Health for the generous help of the precursor and radiolabeling of ¹⁸F-Alfatide II.

Competing Interests

The authors have declared that no competing interest exists.

References

1. Weis SM, Cheresh DA. Tumor angiogenesis: molecular pathways and therapeutic targets. *Nat Med*. 2011;17:1359-70.
2. Abdollahi A, Folkman J. Evading tumor evasion: current concepts and perspectives of anti-angiogenic cancer therapy. *Drug Resist Updat*. 2010;13:16-28.
3. Sessa C, Guibal A, Del CG, Ruegg C. Biomarkers of angiogenesis for the development of antiangiogenic therapies in oncology: tools or decorations? *Nat Clin Pract Oncol*. 2008;5:378-91.
4. Tewari KS, Sill MW, Long HR, Penson RT, Huang H, Ramondetta LM, et al. Improved survival with bevacizumab in advanced cervical cancer. *N Engl J Med*. 2014;370:734-43.
5. Palmer DH. Sorafenib in advanced hepatocellular carcinoma. *N Engl J Med*. 2008;359:2498-9.
6. Raymond E, Dahan L, Raoul JL, Bang YJ, Borbath I, Lombard-Bohas C, et al. Sunitinib malate for the treatment of pancreatic neuroendocrine tumors. *N Engl J Med*. 2011;364:501-13.
7. Rutkowski P, Bylina E, Klimczak A, Switaj T, Falkowski S, Kroc J, et al. The outcome and predictive factors of sunitinib therapy in advanced gastrointestinal stromal tumors (GIST) after imatinib failure - one institution study. *Bmc Cancer*. 2012;12:107.
8. Ebos JM, Kerbel RS. Antiangiogenic therapy: impact on invasion, disease progression, and metastasis. *Nat Rev Clin Oncol*. 2011;8:210-21.
9. Lu-Emerson C, Norden AD, Drappatz J, Quant EC, Beroukhim R, Ciampa AS, et al. Retrospective study of dasatinib for recurrent glioblastoma after bevacizumab failure. *J Neurooncol*. 2011;104:287-91.
10. Kreisl TN, Smith P, Sul J, Salgado C, Iwamoto FM, Shih JH, et al. Continuous daily sunitinib for recurrent glioblastoma. *J Neurooncol*. 2013;111:41-8.
11. Ehling J, Lammers T, Kiessling F. Non-invasive imaging for studying anti-angiogenic therapy effects. *Thromb Haemost*. 2013;109:375-90.
12. Meier R, Braren R, Kosanke Y, Bussemer J, Neff F, Wildgruber M, et al. Multimodality multiparametric imaging of early tumor response to a novel antiangiogenic therapy based on anticalins. *PLoS One*. 2014;9:e94972.
13. Iagaru A, Chen X, Gambhir SS. Molecular imaging can accelerate anti-angiogenic drug development and testing. *Nat Clin Pract Oncol*. 2007;4:556-7.
14. Yang M, Gao H, Yan Y, Sun X, Chen K, Quan Q, et al. PET imaging of early response to the tyrosine kinase inhibitor ZD4190. *Eur J Nucl Med Mol Imaging*. 2011;38:1237-47.
15. Yang M, Gao H, Sun X, Yan Y, Quan Q, Zhang W, et al. Multiplexed PET probes for imaging breast cancer early response to VEGF121/rGel treatment. *Mol Pharm*. 2011;8:621-8.
16. Goggi JL, Bejot R, Moonshi SS, Bhakoo KK. Stratification of ¹⁸F-labeled PET imaging agents for the assessment of antiangiogenic therapy responses in tumors. *J Nucl Med*. 2013;54:1630-6.
17. Bao X, Wang MW, Zhang YP, Zhang YJ. Early monitoring antiangiogenesis treatment response of Sunitinib in U87MG Tumor Xenograft by ¹⁸F-FLT MicroPET/CT imaging. *Biomed Res Int*. 2014;2014:218578.
18. Dumont RA, Hildebrandt I, Su H, Haubner R, Reischl G, Czernin JG, et al. Noninvasive imaging of alphaVbeta3 function as a predictor of the antifibratory and antiproliferative effects of dasatinib. *Cancer Res*. 2009;69:3173-9.
19. Wang MW, Zhang YJ, Zhang YP, Yuan HY. Automated synthesis of hypoxia imaging agent ¹⁸F-FMISO based upon a modified Explora FDG4 module. *J Radioanal Nucl Ch*. 2009;280:149-55.
20. Wang MW, Zhang YP, Zhang YJ. The automated synthesis of ¹⁸F-ML-10 using a microfluidic chip-based synthesizer. *J Nucl Med*. 2014;55:1250.
21. Lang L, Li W, Guo N, Ma Y, Zhu L, Kiesewetter DO, et al. Comparison study of ¹⁸F-FAI-NOTA-PRGD2, ¹⁸F-FPPRGD2, and ⁶⁸Ga-NOTA-PRGD2 for PET imaging of U87MG tumors in mice. *Bioconjug Chem*. 2011;22:2415-22.

22. de Bouard S, Herlin P, Christensen JG, Lemoisson E, Gauduchon P, Raymond E, et al. Antiangiogenic and anti-invasive effects of sunitinib on experimental human glioblastoma. *Neuro Oncol.* 2007;9:412-23.
23. Foote RL, Weidner N, Harris J, Hammond E, Lewis JE, Vuong T, et al. Evaluation of tumor angiogenesis measured with microvessel density (MVD) as a prognostic indicator in nasopharyngeal carcinoma: results of RTOG 9505. *Int J Radiat Oncol Biol Phys.* 2005;61:745-53.
24. Tachibana I, Nishimura Y, Shibata T, Kanamori S, Nakamatsu K, Koike R, et al. A prospective clinical trial of tumor hypoxia imaging with ¹⁸F-fluoromisonidazole positron emission tomography and computed tomography (F-MISO PET/CT) before and during radiation therapy. *J Radiat Res.* 2013;54:1078-84.
25. Wyss MT, Honer M, Schubiger PA, Ametamey SM. NanoPET imaging of [¹⁸F]fluoromisonidazole uptake in experimental mouse tumours. *Eur J Nucl Med Mol Imaging.* 2006;33:311-8.
26. Cheng Z, Wei R, Wu C, et al. Ex-vivo biodistribution and micro-PET/CT imaging of ¹⁸F-FDG, ¹⁸F-FLT, ¹⁸F-FMISO, and ¹⁸F-AIF-NOTA-PRGD2 in a prostate tumor-bearing nude mouse model. *Nucl Med Commun.* 2015;36:914-21.
27. Cheng J, Lei L, Xu J, et al. ¹⁸F-fluoromisonidazole PET/CT: a potential tool for predicting primary endocrine therapy resistance in breast cancer. *J Nucl Med.* 2013;54:333-40.
28. Jain RK. Normalizing tumor vasculature with anti-angiogenic therapy: a new paradigm for combination therapy. *Nat Med.* 2001;987-9.
29. Jain RK. Normalization of tumor vasculature: an emerging concept in antiangiogenic therapy. *Science.* 2005;307:58-62.
30. Cohen A, Shirvan A, Levin G, Grimberg H, Reshef A, Ziv I. From the Gla domain to a novel small-molecule detector of apoptosis. *Cell Res.* 2009;19:625-37.
31. Hoglund J, Shirvan A, Antoni G, Gustavsson SA, Langstrom B, Ringheim A, et al. ¹⁸F-ML-10, a PET tracer for apoptosis: first human study. *J Nucl Med.* 2011;52:720-5.
32. Oborski MJ, Laymon CM, Lieberman FS, Drappatz J, Hamilton RL, Mountz JM. First use of ¹⁸F-labeled ML-10 PET to assess apoptosis change in a newly diagnosed glioblastoma multiforme patient before and early after therapy. *Brain Behav.* 2014;4:312-5.
33. Wang MW, Wang F, Zheng YJ, Zhang YJ, Zhang YP, Zhao Q, et al. An in vivo molecular imaging probe ¹⁸F-Annexin B1 for apoptosis detection by PET/CT: preparation and preliminary evaluation. *Apoptosis.* 2013;18:238-47.
34. Zeng W, Wang X, Xu P, Liu G, Eden HS, Chen X. Molecular imaging of apoptosis: from micro to macro. *Theranostics.* 2015;5:559-82.
35. Lederle W, Arns S, Rix A, Gremse F, Doleschel D, Schmaljohann J, et al. Failure of annexin-based apoptosis imaging in the assessment of antiangiogenic therapy effects. *EJNMMI Res.* 2011;1:26.
36. Kishino T, Hoshikawa H, Nishiyama Y, Yamamoto Y, Mori N. Usefulness of 3'-deoxy-³-¹⁸F-fluorothymidine PET for predicting early response to chemoradiotherapy in head and neck cancer. *J Nucl Med.* 2012;53:1521-7.
37. Inubushi M, Saga T, Koizumi M, Takagi R, Hasegawa A, Koto M, et al. Predictive value of 3'-deoxy-³-¹⁸F-fluorothymidine positron emission tomography/computed tomography for outcome of carbon ion radiotherapy in patients with head and neck mucosal malignant melanoma. *Ann Nucl Med.* 2013;27:1-10.
38. Hoeben BA, Troost EG, Span PN, van Herpen CM, Bussink J, Oyen WJ, et al. ¹⁸F-FLT PET during radiotherapy or chemoradiotherapy in head and neck squamous cell carcinoma is an early predictor of outcome. *J Nucl Med.* 2013;54:532-40.
39. Saint-Hubert MD, Brepoels L, Devos E, Vermaelen P, Groot TD, Tousseyen T, et al. Molecular imaging of therapy response with ¹⁸F-FLT and ¹⁸F-FDG following cyclophosphamide and mTOR inhibition. *Am J Nucl Med Mol Imaging.* 2012;2:110-21.
40. Zhu Z, Miao W, Li Q, Dai H, Ma Q, Wang F, et al. ^{99m}Tc-3PRGD2 for Integrin Receptor Imaging of Lung Cancer: A Multicenter Study. *J Nucl Med.* 2012;53:716-22.
41. Battle MR, Goggi JL, Allen L, Barnett J, Morrison MS. Monitoring tumor response to antiangiogenic sunitinib therapy with ¹⁸F-flucilatide, an ¹⁸F-labeled alphaVbeta3-integrin and alphaV beta5-integrin imaging agent. *J Nucl Med.* 2011;52:424-30.
42. Wan W, Guo N, Pan D, Yu C, Weng Y, Luo S, et al. First experience of ¹⁸F-alfatide in lung cancer patients using a new lyophilized kit for rapid radiofluorination. *J Nucl Med.* 2013;54:691-8.
43. Mi B, Yu C, Pan D, Yang M, Wan W, Niu G, et al. Pilot prospective evaluation of ¹⁸F-alfatide II for detection of skeletal metastases. *Theranostics.* 2015;5:1115-21.
44. Liu Z, Jia B, Shi J, Jin X, Zhao H, Li F, et al. Tumor Uptake of the RGD Dimeric Probe ^{99m}Tc-G3-2P4-RGD2 is Correlated with Integrin αvβ3 Expressed on both Tumor Cells and Neovasculature. *Bioconjugate Chem.* 2010;21:548-55.
45. Gao L, Liu H, Sun X, Gao D, Zhang C, Jia B, et al. Molecular imaging of post-Src-inhibition tumor signatures for guiding dasatinib combination therapy. *J Nucl Med.* 2016;57:321-6.